Journal of Building Engineering 117 (2026) 114554

Contents lists available at ScienceDirect

Journal of Building Engineering

journal homepage: www.elsevier.com/locate/jobe

Innovative reinforced aluminium alloy curtain walls: Numerical analysis and experimental validation

Antonio Formisano [a,*], Muhammad Tayyab Naqash [b,**]

[a] Department of Structures for Engineering and Architecture, University of Naples Federico II, Naples, Italy
[b] Department of Civil Engineering, Faculty of Engineering, Islamic University of Madinah, Madinah, Kingdom of Saudi Arabia

ARTICLE INFO

Keywords:
Aluminium curtain walls
Composite system
Reinforced profiles
Experimental testing
Numerical analysis
Structural performance

ABSTRACT

Aluminium curtain walls are a prevalent choice for the building facade due to their lightweight nature, corrosion resistance, and aesthetic qualities. However, the high deformability of aluminium alloys poses challenges in meeting serviceability requirements under wind and seismic loads, particularly building sway. This study investigates a novel reinforced aluminium curtain wall profile designed to overcome these limitations.

The research introduces an innovative prestressed aluminium alloy profile, internally reinforced with tensioned steel cables. Both numerical simulations and experimental validation are presented. Multiple reinforcement configurations are analyzed to determine the optimal arrangement for enhancing stiffness and structural strength. Nonlinear finite element analyses, conducted using ABAQUS, assess the sensitivity to the number and placement of reinforcing cables. The most effective configuration identified through simulation is selected for subsequent experimental testing.

Results: from the simulations indicate up to an 86 % reduction in deflection compared to conventional aluminium profiles. Experimental validation showed a 5 % increase in structural stiffness, confirming the effectiveness of the proposed reinforcement system. These enhancements in lateral drift control and load-bearing capacity demonstrate the potential of the proposed solution to balance structural performance.

1. Introduction

Aluminium alloy profiles are extensively used in modern curtain wall systems due to their lightweight, corrosion resistance, and aesthetic versatility. However, their relatively high deformability presents challenges in resisting building sway induced by wind and seismic forces. To address these limitations, a novel prestressed aluminium alloy profile reinforced with tensioned steel cables has been developed [1,2].

Curtain walls, as non-structural exterior envelopes, serve critical roles in resisting air and water infiltration, withstanding wind pressures, and allowing natural light transmission. In regions prone to extreme weather, properly engineered curtain walls help mitigate risks such as glass breakage, thus preserving the integrity of the building envelope and minimizing interior damage. Contemporary architectural design adds complexity to facade engineering, requiring solutions that balance structural performance

* Corresponding author.
** Corresponding author.
E-mail addresses: antoform@unina.it (A. Formisano), engr.tayyabnaqash@gmail.com (M.T. Naqash).

https://doi.org/10.1016/j.jobe.2025.114554
Received 8 July 2025; Received in revised form 9 October 2025; Accepted 2 November 2025
Available online 19 November 2025

with cultural and aesthetic preservation [3,4].

Modern materials and techniques, particularly aluminium-based systems, are increasingly being adopted in building facade. For example, aluminium's light weight, corrosion resistance, and adaptability make it well-suited for retrofitting fragile historical structures that may not support heavier cladding materials [5,6]. Nevertheless, the inherent deformability of aluminium alloys complicates compliance with serviceability requirements, especially under lateral loads such as wind [7].

Research has shown that aluminium curtain walls often experience excessive lateral drift when subjected to wind and seismic forces [8–10], emphasizing the need for innovative reinforcement strategies that maintain architectural integrity. Several studies [11–13] highlight the importance of accurately characterizing aluminium's mechanical response under various loading conditions to develop designs that satisfy safety and performance standards. With the growing prevalence of high-rise construction in urban areas, curtain wall systems have also become integral to achieving improved thermal efficiency and overall building energy performance [14,15].

This study investigates a novel reinforced aluminium curtain wall profile aimed at overcoming the limitations associated with the high deformability of aluminium alloys. It introduces an innovative prestressed aluminium alloy profile internally reinforced with tensioned steel cables. A range of reinforcement configurations is examined to determine the optimal arrangement for maximizing both stiffness and structural strength. Nonlinear finite element analyses were conducted using the ABAQUS software to assess the system's sensitivity to variations in the number and placement of cables. The most effective configuration identified through these simulations will subsequently undergo experimental validation [16,17].

The numerical results reveal substantial enhancements in key performance metrics, including lateral drift control and load-bearing capacity. In particular, the reinforced profiles achieved up to an 86 % reduction in deflection compared to standard, non-reinforced aluminium profiles. These findings contribute to the advancement of high-performance curtain wall systems that successfully balance structural demands with the architectural preservation of historical buildings [18].

This approach builds on the work of [19], who explored composite aluminium–steel profiles for curtain wall applications, drawing on design solutions offered by various commercial manufacturers (see Fig. 1). Their research underscores the potential of hybrid material systems in improving the mechanical performance of facade components.

A common feature of all the reinforcement solutions illustrated in Fig. 1 is that the steel reinforcement is not mechanically connected to the base aluminium profile. Instead, these systems operate as hybrid assemblies made of a simple coupling of profiles made from two distinct materials. One of the primary motivations for developing combined aluminium–steel systems in curtain wall applications is to improve the structural performance of aluminium alloy sections by reducing their inherent deformability under applied loads.

When aluminium is used as the primary structural material, its metallurgical advantages, such as ease of extrusion along with its corrosion resistance, low specific weight, and aesthetic qualities (e.g., anodization), make it a preferred choice. However, its relatively low elastic modulus presents a disadvantage, particularly for vertical mullions or other members subjected primarily to bending. To address this, incorporating steel profiles alongside aluminium can significantly enhance stiffness, owing to the much higher elastic modulus of steel [20].

Recent research has increasingly focused on reinforcement strategies for aluminium profiles, particularly through the use of tensioned steel cables. Numerical studies by the authors [21] have demonstrated that such prestressed aluminium profiles can achieve markedly improved stiffness and load-bearing capacity. These findings offer promising implications for modern curtain wall systems and in applications involving the restoration of facades where both structural performance and preservation are critical.

The integration of steel inserts as stiffeners to control deflection is now a well-established practice in curtain wall design [22]. For instance, Technal curtain walling products [23] incorporate steel reinforcements while maintaining a high level of aesthetic quality and durability. These systems combine advanced manufacturing methods with innovative engineering features to ensure reliable installation and long-term performance. In particular design cases, the depth of the mullion may be either excessive, visually protruding beyond the facade, or insufficient to satisfy deflection criteria. In such instances, aluminium mullions are reinforced with internal steel stiffeners, as illustrated in Fig. 2. Similarly, when transom sections are inadequate to support the dead load of glazing elements, they too are often reinforced with steel to meet structural requirements.

An important factor to consider in the design of combined aluminium–steel profiles is the influence of temperature variations. While the effect of thermal expansion in systems combining materials with similar coefficients, such as different steel types, is

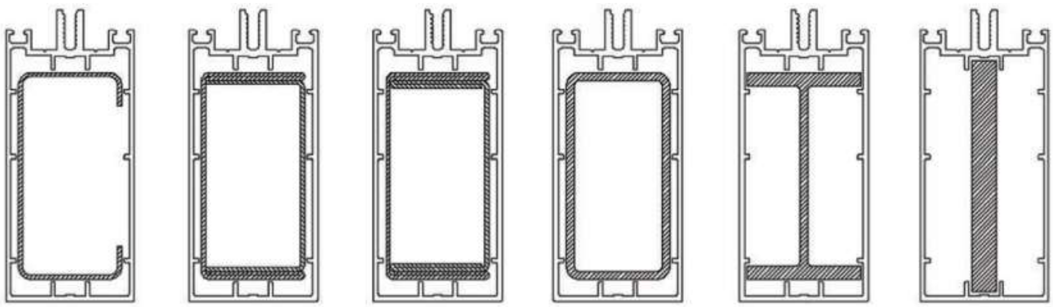

Fig. 1. Examples of steel reinforcements for aluminium profiles of curtain wall systems.

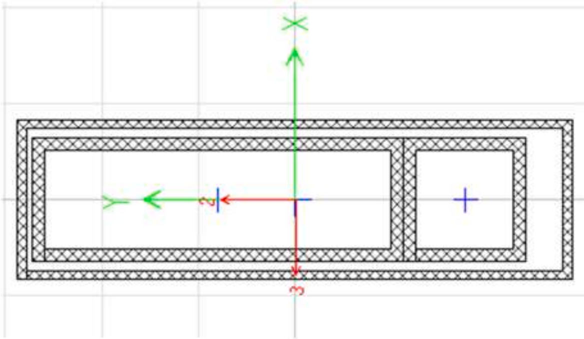

Fig. 2. Mullion profile with stiffeners to control deflection.

generally negligible, the disparity becomes significant in aluminium–steel assemblies. Specifically, aluminium exhibits a thermal expansion coefficient of approximately $\alpha_a = 2.3 \times 10^{-5}\,^{\circ}C^{-1}$, nearly double that of steel, which is $\alpha_s = 1.2 \times 10^{-5}\,^{\circ}C^{-1}$. This substantial difference can induce thermal stresses and differential deformation under temperature fluctuations, which may compromise long-term performance or induce serviceability issues. Despite its significance, this physical phenomenon is often overlooked in the existing literature, including in several studies previously cited [24–26].

Another limitation in current research and design practice is the lack of standardized guidelines for such hybrid systems. The final version of the European code for aluminium structures, namely the Eurocode 9, Part 1.1 [26] omits provisions related to aluminium–steel composite systems, which had been included in earlier drafts. As a result, designers face challenges in the structural verification of these assemblies due to the absence of a codified design methodology.

In facade systems, connections between aluminium and steel profiles are commonly made using self-drilling screws at the interface between transoms and mullions. In the absence of a fully composite section, the mechanical analysis of such systems can be simplified by assuming that the aluminium and steel profiles deform compatibly, that is, they share a typical curvature or strain. For instance, under a uniformly distributed load applied to a beam composed of aluminium and steel elements, the global response can be analyzed using composite beam theory. In such a case, the governing relationship may be expressed as follows [19]:

$$q_s = q\left(\frac{3\frac{I_s}{I_a}}{1+3\frac{I_s}{I_a}}\right) \textit{ respectively}, q_a = q\left(1-\frac{3\frac{I_s}{I_a}}{1+3\frac{I_s}{I_a}}\right) \tag{1}$$

Using Eq. (1), it is possible to determine the load share carried by aluminium (q_a) or steel (q_s). The underlying relationships assume a constant ratio between the elastic moduli of the two materials, with $E_s = 210{,}000$ MPa for steel and $E_a = 70{,}000$ MPa for aluminium, yielding a ratio $E_s/E_a = 3$. The terms I_a and I_s refer to the moments of inertia of the aluminium and steel sections, respectively.

One of the key motivations for pursuing combined aluminium–steel profiles in curtain wall design is to enhance the mechanical performance of conventional aluminium sections, particularly in reducing their excessive deformability under service loads. Aluminium alloys are widely used due to their advantageous characteristics: excellent extrudability, high corrosion resistance, low specific weight, and aesthetic flexibility (e.g., anodization). However, their reduced elastic modulus becomes a critical limitation, especially in vertical mullions or other components predominantly subjected to bending. The integration of steel sections, thanks to their significantly higher stiffness, can compensate for this shortcoming and substantially reduce the deformation of the hybrid system [27].

Despite the clear structural benefits, the implementation of such composite profiles is hindered by the absence of dedicated design standards. The final version of Eurocode 9, Part 1.1 (European Union, 2007), which governs aluminium structures, no longer includes provisions for aluminium–steel composite systems, which were instead present in earlier drafts. This regulatory gap complicates design validation and limits the widespread adoption of these innovative systems.

Another crucial consideration is the effect of temperature variations on hybrid profiles. In composite steel–concrete systems, thermal expansion is typically negligible due to the similar thermal coefficients of the constituent materials. However, aluminium–-steel combinations exhibit one of the most significant thermal expansion coefficients as given by Equation (2), among commonly used structural materials. Specifically, aluminium has a coefficient of thermal expansion $\alpha_a = 2.3 \times 10^{-5}\,^{\circ}C^{-1}$, nearly double that of steel ($\alpha_s = 1.2 \times 10^{-5}\,^{\circ}C^{-1}$).

$$\alpha = \left(\frac{\frac{\Delta L}{L}}{\Delta T}\right) \tag{2}$$

α Coefficient of linear thermal expansion (in $^{\circ}C^{-1}$ or K^{-1})
ΔT Change in temperature (in °C or K)
ΔL Change in length of the material.

L Original length of the material.

This discrepancy leads to significant internal stresses during temperature fluctuations. Upon heating, the aluminium component naturally tends to expand more than the steel. However, to maintain strain compatibility (i.e., equal elongation), the aluminium undergoes compressive stress. At the same time, the steel is subjected to tensile stress. The opposite effect occurs during cooling, with aluminium in tension and steel in compression.

Assuming the composite bar is unrestrained externally and subjected only to thermal loading, the internal forces in the aluminium and steel components must be in equilibrium. By equating the formulas for the elongation at break of the aluminium and steel components, it is possible to analytically determine the ultimate elongation, ε_i, of the composite bar due to temperature variation ΔT_u, as well as the stresses occurring in the aluminium (σ_a) and the steel (σ_s). These expressions are presented in the following equation (3) [28]:

$$\varepsilon_i = \Delta T_u\left(\frac{\alpha_a A_a E_a + \alpha_s A_s E_s}{A_a E_a + A_s E_s}\right), \quad \sigma_a = \Delta T_u(\alpha_a - \alpha_s)\left(\frac{E_a A_s E_s}{A_a E_a + A_s E_s}\right), \quad \sigma_s = \Delta T_u(\alpha_s - \alpha_a)\left(\frac{E_s A_a E_a}{A_a E_a + A_s E_s}\right) \tag{3}$$

By treating the elastic moduli and thermal expansion coefficients of aluminium alloys and steel as constants, one can derive, through appropriate mathematical transformations, Eq. (4). This Equation enables the calculation of the effective thermal expansion coefficient (α_i) of the idealized composite section. Additionally, it allows for the determination of the thermally induced stresses in both the steel and aluminium components, expressed as functions of the ratio between the cross-sectional areas of steel (A_s) and aluminium (A_a).

$$\alpha_i = \left(\frac{\alpha_a A_a E_a + \alpha_s A_s E_s}{A_a E_a + A_s E_s}\right) = \alpha_i\left[\frac{1 + 1,565\frac{A_s}{A_a}}{1 + 3\frac{A_s}{A_a}}\right], \quad |\sigma_a| = 2,31 \times |\Delta T_u|\left(\frac{\frac{A_s}{A_a}}{1 + 3\frac{A_s}{A_a}}\right) \;\; in \;\; [Mpa], \quad |\sigma_s|$$
$$= 2,31 \times |\Delta T_u|\left(\frac{1}{1 + 3\frac{A_s}{A_a}}\right) \;\; in \;\; [Mpa] \tag{4}$$

Therefore, the variable chosen during the design phase is the ratio between the areas of the two materials, i.e. A_s/A_a, in Eq. (4) the stresses and temperature variations are considered as absolute values. The A_s/A_a ratio may vary within the range [0.1–0.8], as lower values could complicate the feasibility of the composite section. In comparison, higher values may indicate a reinforced steel profile rather than a reinforced aluminium one.

Using the range [0.001–1000] for A_s/A_a and Eq. (3) [19], plotted the relative stress diagrams $\sigma_{i,\Delta Tu}/f_{i,y}$ as a function of the variable A_s/A_a on a logarithmic scale, as illustrated in Fig. 3.

The above diagram leads to the conclusion that for the actual pair of materials used, i.e., 6060-T6 aluminium alloy and S355 steel, and for usual temperature variations in the structural engineering sector ($\Delta T_u = \pm$ 15–50 °C), neither of the two materials can be exhausted. Therefore, an optimal range of the cross-sectional area ratio A_s/A_a of the composite cross-section materials is contained in the range [0.1–0.8].

To achieve these objectives, a systematic approach combining numerical modeling and experimental validation was implemented, as described in the following section. The proposed methodology was developed to evaluate the mechanical performance of the reinforced profiles under realistic loading conditions.

2. Methodology

The prestressing technique is based on a straightforward concept: applying loads to a structure in a way that enables it to resist significantly larger loads. Prestressing methods, including the use of tensioned steel cables, have been proposed to improve the performance of aluminium alloy profiles in curtain wall systems. By reducing deflections and increasing the stiffness and strength of the profiles, prestressing allows them to withstand wind and seismic forces better.

The mechanical behavior of the examined profile, referred to as the M0 profile, was analyzed using the finite element software

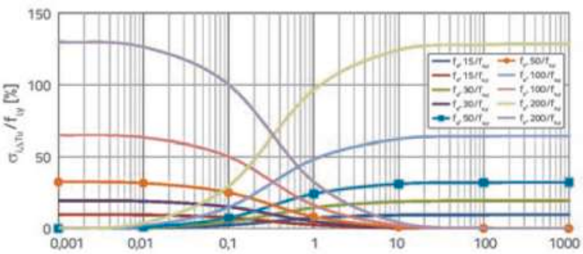

Fig. 3. Stresses related to the combined profile composed of AW6060-T5 aluminium alloy and S355 steel.

ABAQUS CAE 6.14–4 [29]. Three hypotheses were tested to enhance the prestressing system's performance and optimize the steel wire configuration under wind and earthquake loads.

Surface-to-surface contact definitions were applied to represent the interaction between bolts and surrounding aluminium plates accurately. A hard contact formulation was used in the normal direction to prevent penetration, while penalty-based frictional contact was defined in the tangential direction, simulating realistic shear transfer. The bolt holes were explicitly modeled, and preload effects were introduced using ABAQUS pretension sections to simulate the clamping action of bolts. This approach ensured a realistic representation of the load transfer mechanism at the steel–aluminium interface.

This comprehensive simulation setup provides a solid foundation for evaluating the effectiveness of the proposed prestressed wire reinforcement systems. Careful selection of the mesh and boundary conditions ensures that the numerical results accurately represent the physical behavior of the aluminium profile, enabling meaningful comparisons between the unreinforced profile and various reinforcement configurations (M1, M2, and M3) discussed in the subsequent section of the numerical analysis. The selected solution involves using four straight harmonic steel cables, tensioned through specially designed rope-holding systems.

This study focuses on an AW-6060 T5 extruded aluminium alloy profile [30] commonly used in mullion and transom curtain wall systems. The aim is to enhance the profile's performance by integrating a prestressed steel system designed to minimize displacements under lateral loads. The aluminium alloy (AW-6060 T5) was modeled using an elastic-perfectly plastic constitutive law with a Young's modulus of 70 GPa and a yield stress of 120 MPa. The steel cables were modeled using a bilinear isotropic hardening model with an initial modulus of 210 GPa, yield stress of 1530 MPa, and post-yield modulus of 1 GPa.

The basic aluminium alloy profile is shown in Fig. 4(a), with its geometric dimensions detailed in Fig. 4(b). The profile has a cross-section measuring 110 mm × 50 mm, where the 50 mm represents the visible width on the front elevations of standard curtain wall systems. It weighs 2.827 kg/m, has a second moment of area of 192.24 cm^4 about the strong axis, and a total length of 3000 mm. Manufactured from an aluminium-magnesium-silicon alloy, this material is easily extruded, allowing for the production of profiles with complex cross-sections. The mechanical properties of the alloy are as follows: conventional yield strength $f_{0.2} = 120$ MPa, ultimate strength $f_u = 160$ MPa, and ultimate deformation $A_{50} = 8$ %.

Design considerations play a crucial role in this study, addressing both architectural constraints and compliance with current building codes and standards. The study's methodology is briefly outlined in Fig. 5. Additionally, the research emphasizes simplifying maintenance and installation processes while ensuring seamless integration of curtain walls with other building components, particularly structural restorations, to achieve optimal performance and functionality [4].

Based on the outlined methodology, a detailed numerical analysis was carried out to evaluate the structural behavior of the reinforced aluminium profiles. The following section presents the results obtained from the finite element simulations, highlighting the comparative performance of the different reinforcement configurations.

3. Numerical analysis

Three strengthening interventions have been applied to the basic profile to enhance its stiffness under load. The system typically uses rope supports to secure the prestressed harmonic steel cables with wedges. To accurately simulate the mechanical connections, the interaction between the bolts and the surrounding aluminium plates was explicitly defined. A surface-to-surface contact was applied with hard contact in the normal direction and frictional behavior in the tangential direction. Bolt holes were modeled as three-dimensional voids, and bolt preload was introduced using pretension elements in ABAQUS. Various anchoring methods and cable configurations have been explored, resulting in three proposed designs: M1, M2, and M3.

The first design, specimen M1, employs steel grade S275 for rope supports attached to the ends of the aluminum profile using four countersunk TSPEI screws, as illustrated in Fig. 6. This figure presents detailed technical drawings of the M1 composite specimen and its critical connection components. Fig. 6(a) shows a cross-sectional view of the complete M1 assembly, highlighting the integration of the reinforcement system with the aluminum profile, which has an overall width of 110 mm. The TSPEI screws (countersunk with hexagonal sockets) secure the rope supports to the aluminum profile's side, with their placement being crucial for effective load transfer between the profile and the reinforcement.

Fig. 6(b) provides multiple detailed views of the rope support component, emphasizing its key features.

- Holes for 4 mm diameter wire: These precisely sized openings accommodate the steel cables that provide reinforcement. The 4 mm diameter specification ensures proper fit and alignment of the reinforcing elements.

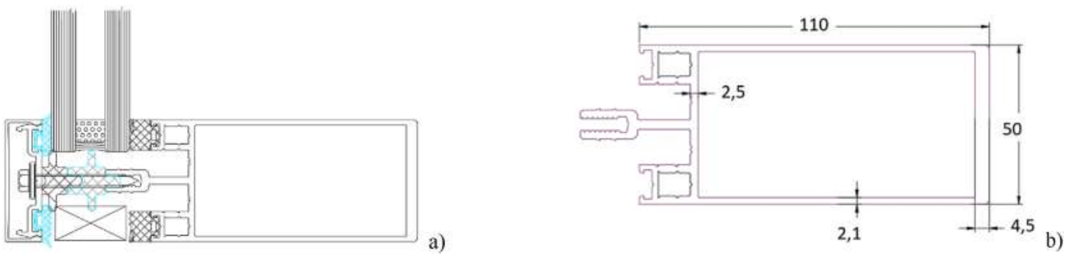

Fig. 4. Graphical representation (a) and geometrical dimensions (b) of the aluminium alloy profile under study.

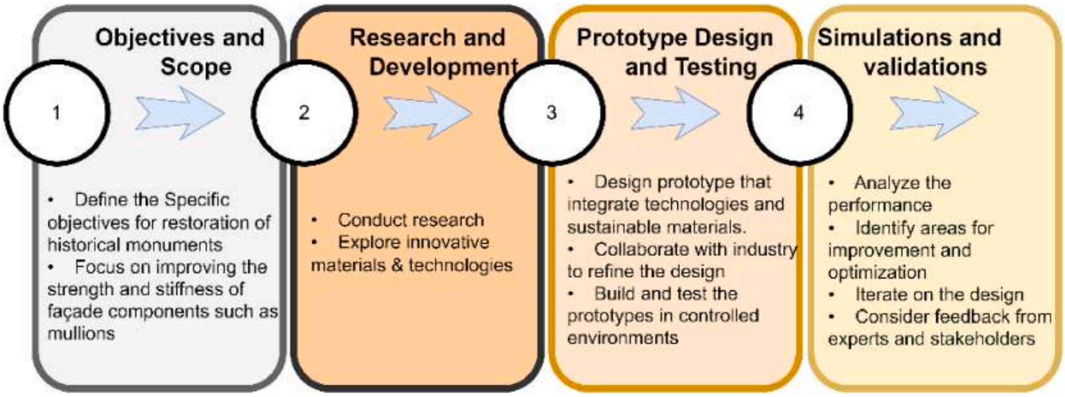

Fig. 5. Innovative prestressed aluminium profile.

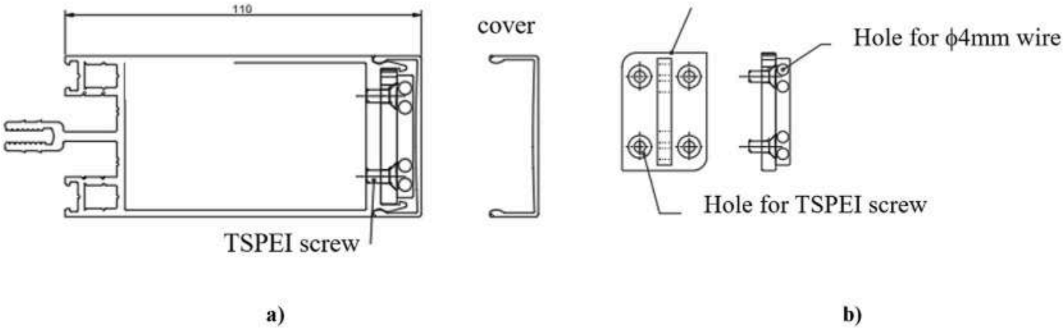

Fig. 6. The specimen M1: configuration (a) and details (b).

- Holes for TSPEI screws: These allow for mechanical fastening of the rope support to the aluminum profile.
- Cover: A cover component is included, likely to protect the connection and add stability to the assembly.

The detailed engineering drawings reflect a thoughtful design approach for the M1 configuration. The rope supports are strategically positioned at the profile's corners to maximize the mechanical advantage of the tensioned cables. The 4 mm diameter specification for the reinforcing cables strikes a careful balance between meeting strength requirements and practical size constraints.

These technical details illustrate the precision engineering essential for the successful implementation of the prestressed composite system. The fastening method using TSPEI screws offers a straightforward and effective connection. However, performance data indicate that this approach is less effective than the through-bolt clamping mechanism employed in the M2 configuration.

Each rope support features four 4 mm-diameter holes to accommodate the steel cables. The supports are fabricated from harmonic steel, with nominal yield and ultimate strengths of 1530 MPa and 1730 MPa, respectively. After prestressing, the cables are secured with anchor wedges. Although these wedges are not explicitly modeled in the software for simplicity, their effect is represented through appropriate support boundary conditions.

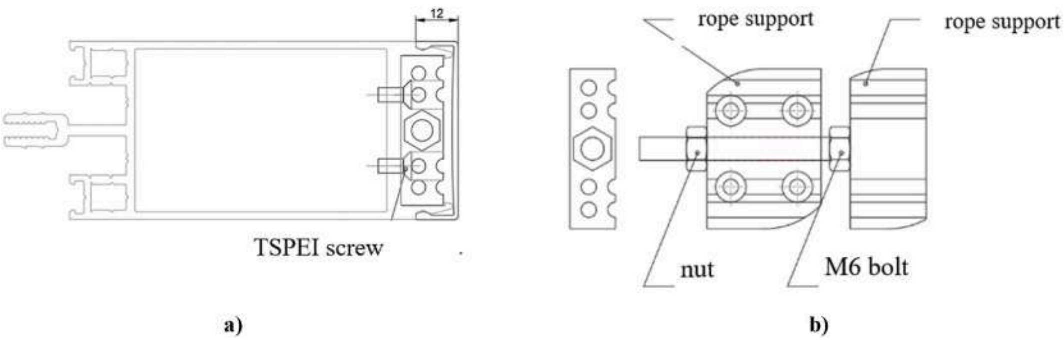

Fig. 7. Configuration (a) and details (b) of the M1 and M2 reinforcement systems.

The second configuration, specimen M2, is similar to M1 but employs a different rope support geometry, as shown in Fig. 7. This design includes a central M6 bolt that is tightened to secure the connection to the aluminum profile [20].

Fig. 7 illustrates the technical drawings detailing the connections for the M1 and M2 reinforcement configurations, providing essential insight into how the rope supports are secured to the aluminum profiles.

Fig. 7(a) presents the details of the connection for the M1 configuration. The cross-sectional drawing shows the rope support attached to the side of the aluminum profile using TSPEI screws (countersunk screws with hexagonal sockets). This fastening method

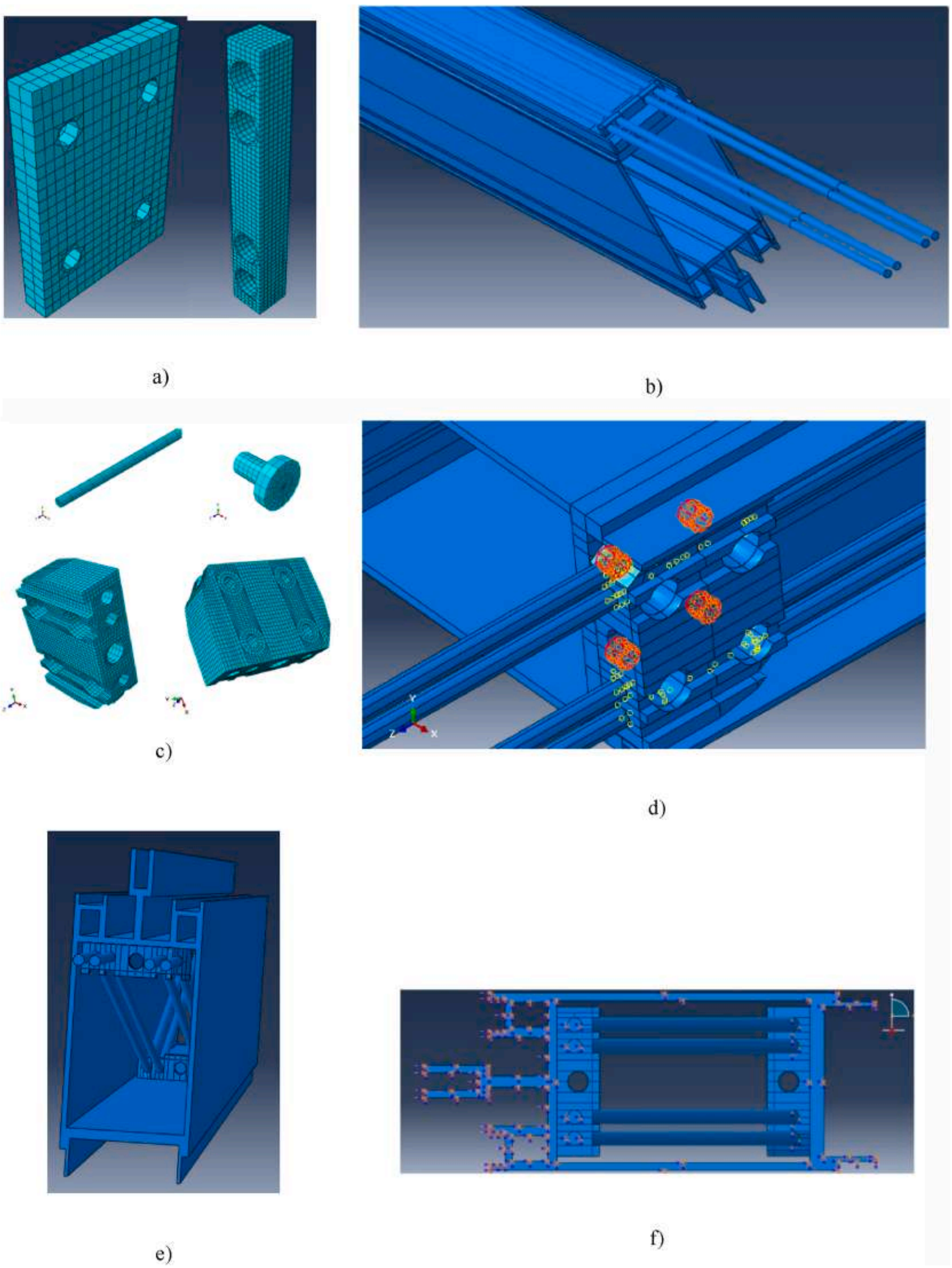

Fig. 8. Detailed numerical models of the three proposed reinforcement configurations (M1, M2, and M3) developed in the ABAQUS finite element analysis environment.

offers a clean, flush finish while ensuring a secure attachment. The 12 mm dimension at the top indicates the width of the connection component. The rope support includes several circular openings designed to accommodate the steel cables. This configuration depends on the mechanical fastening of the rope support to transfer forces between the cables and the aluminum profile.

Fig. 7(b) depicts the connection detail for the M2 configuration, which features a more robust attachment system. The drawing includes front and side views of the connection, labeling components such as the "rope supports," "nut" and "M6 bolt." The M2 configuration uses an M6 bolt that passes through the rope support and is secured with a nut on the opposite side, creating a clamping effect that enhances connection stability. In the M1 and M2 configurations, rope supports were mechanically connected to the aluminium profile using TSPEI screws (in M1) and clamping bolts (in M2). To simulate these connections accurately, the interaction between the bolts and the surrounding aluminium plates was explicitly modeled in the finite element setup. A surface-to-surface contact was defined between the bolt shank and the hole surfaces, with hard contact in the normal direction to prevent penetration and penalty-based frictional contact in the tangential direction to simulate realistic shear transfer. The bolt holes were modeled explicitly in the aluminium geometry, and bolt preload effects were introduced using ABAQUS *pretension sections*, allowing the simulation to capture the clamping effect and its contribution to load transfer and stiffness. This modeling approach ensured a realistic representation of the load path and local stress distribution, particularly at the steel–aluminium interface in configurations M1 and M2. Similar to M1, the rope support contains multiple circular openings for the steel cables, positioned to optimize force transfer.

The key distinction between these connection methods lies in their mechanical principles: M1 relies on the shear strength of the TSPEI screws, while M2 employs a through-bolt clamping mechanism. This difference likely explains the superior performance of M2 observed in the numerical analysis, as the clamping mechanism provides more consistent force transfer between the tensioned cables and the aluminum profile. These detailed drawings underscore the careful engineering considerations involved in designing the reinforcement systems, emphasizing not only the theoretical performance of the tensioned cables but also their practical integration with the aluminum profiles.

The third configuration, specimen M3, uses the same rope support as M2 but arranges the harmonic steel cables in a parabolic shape. To achieve this geometry, two rope supports are positioned at the profile's ends, with an additional support located at the midpoint to guide the cable and form the parabolic curve. Numerical models of the three steel wire–aluminium profile composite configurations, developed using Abaqus software, are illustrated in Fig. 8 [31,32].

Fig. 8(a) and (b) illustrate the M1 configuration. Fig. 8(a) shows the mesh structure of the rope support components from two different angles, with the turquoise color representing the finite element discretization used for precise stress and deformation analysis. The circular holes visible in the rope supports are designed to accommodate the steel cables. Fig. 8(b) provides a three-dimensional view of the complete M1 assembly, where the blue components represent the aluminum profile, and the integrated steel cables run parallel to the profile's longitudinal axis.

Fig. 8(c) and (d) depict the M2 configuration. Fig. 8(c) presents the meshed components of the M2 system, including the modified rope support with its central bolt connection and the individual elements forming the assembly. Fig. 8(d) offers a detailed view of the connection between the rope supports and the aluminum profile. The colored elements differentiate the components of the assembly: orange likely indicates fasteners or connection points. In contrast, the multicolored elements illustrate the interface between the steel cables and the rope supports.

Fig. 8(e) and (f) show the M3 configuration, featuring the distinctive parabolic wire arrangement. Fig. 8(e) provides a cross-sectional view of the aluminum profile with its internal structure designed to accommodate the parabolic cable path. The unique geometry necessary to guide the cables along a curved trajectory is clearly visible. Fig. 8(f) offers a top view of the M3 system, highlighting the layout of connection points, indicated by red markers that establish the parabolic trajectory of the reinforcing cables.

The detailed modeling of these configurations enabled precise analysis of stress distribution, deformation patterns, and overall structural behavior under applied loads. The refined mesh ensured accurate capture of localized effects, especially at connection points between different materials and components. These numerical models were crucial for evaluating the relative performance of each reinforcement strategy and identifying the most effective configuration (M2) prior to physical prototyping and testing.

The level of detail in these models exemplifies the comprehensive approach taken during the numerical analysis phase, providing a solid foundation for subsequent experimental validation of the most promising reinforcement design.

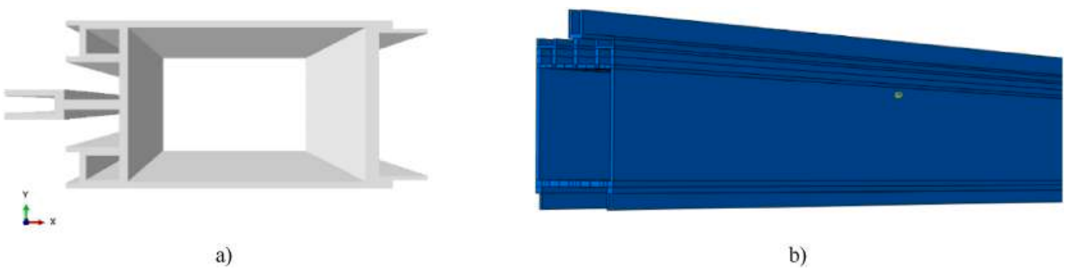

Fig. 9. Cross-section (a) and 3D view (b) of the used aluminium alloy profile.

3.1. Baseline performance of unreinforced profiles

ABAQUS was used to develop a numerical model of the aluminum profile. Fig. 9 presents a 3D model of the aluminum alloy member, constructed using solid elements.

Fig. 9 presents the core aluminum alloy profile that serves as the foundation for the reinforcement study, showcasing both its cross-sectional details and three-dimensional form as modeled in ABAQUS.

Fig. 9(a) displays the cross-sectional geometry of the aluminum profile. Rendered in light gray, it reveals a complex internal structure featuring a hollow rectangular core with multiple chambers and reinforcing webs. The design includes two main hollow chambers separated by a central vertical web, with additional horizontal webs strengthening the top and bottom flanges. Specialized edge geometries provide mounting surfaces and enhance rigidity. This sophisticated cross-section is engineered to maximize the moment of inertia while minimizing material usage, exemplifying efficient aluminum extrusion design. The coordinate system at the lower left indicates that the Y-axis represents the vertical direction along which loads are applied.

Fig. 9(b) shows the three-dimensional solid model of the aluminum profile as implemented in ABAQUS. The blue-rendered model extends the cross-section along its longitudinal axis, creating the beam-like element studied for reinforcement. Constructed using solid elements rather than shell elements, this approach allows precise representation of the profile's complex geometry. It facilitates accurate stress analysis throughout the material volume. This ensures that localized stress concentrations and three-dimensional deformation behaviors are effectively captured in the numerical simulation.

Before finalizing the mesh size for the simulation, a mesh sensitivity analysis was conducted to ensure the balance between computational efficiency and result accuracy. Three different element sizes were tested: 10 mm, 7.5 mm, and 5 mm. The results showed that while the coarser meshes led to faster computations, they introduced noticeable variations in peak deflection values and local stress concentrations. The **5** mm mesh was found to provide stable and accurate results without excessive computational cost. Therefore, it was selected for all subsequent simulations. This mesh size was particularly effective in capturing local effects at stress concentration points such as bolt connections and the steel–aluminium interface.

The detailed geometric representation of the aluminum profile is critical for subsequent analyses, providing the baseline structure for the various reinforcement configurations. The complex cross-section with multiple chambers poses specific challenges and opportunities for integrating the steel wire reinforcement systems, particularly regarding optimal wire anchoring and routing. Accurate modeling of this geometry is essential for establishing valid comparisons between the unreinforced profile and the reinforced variants.

This aluminum alloy profile typifies structural elements used in architectural and industrial applications, where a high strength-to-weight ratio and design flexibility are key considerations. Restraint conditions were applied after defining the geometry and assigning physical and mechanical properties to the profile components. Since the uprights and transoms are typically bolted together, the profile was secured at both ends using spherical hinges. The specimen was subjected to a uniformly distributed load corresponding to a pressure of p = 0.001355 MPa, reflecting the highest wind zone specified by the Italian Technical Standard NTC 2018 [33,34].

Regarding mesh size, a preliminary sensitivity study identified a side length of 5 mm as the optimal balance between computational efficiency and result accuracy, as shown in Fig. 10(a). The profile is supported at both ends, with the uniformly distributed load applied on the top surface, as illustrated in Fig. 4(b). The maximum deflection under this load is 0.134 mm, with the deformed shape shown in Fig. 10(c).

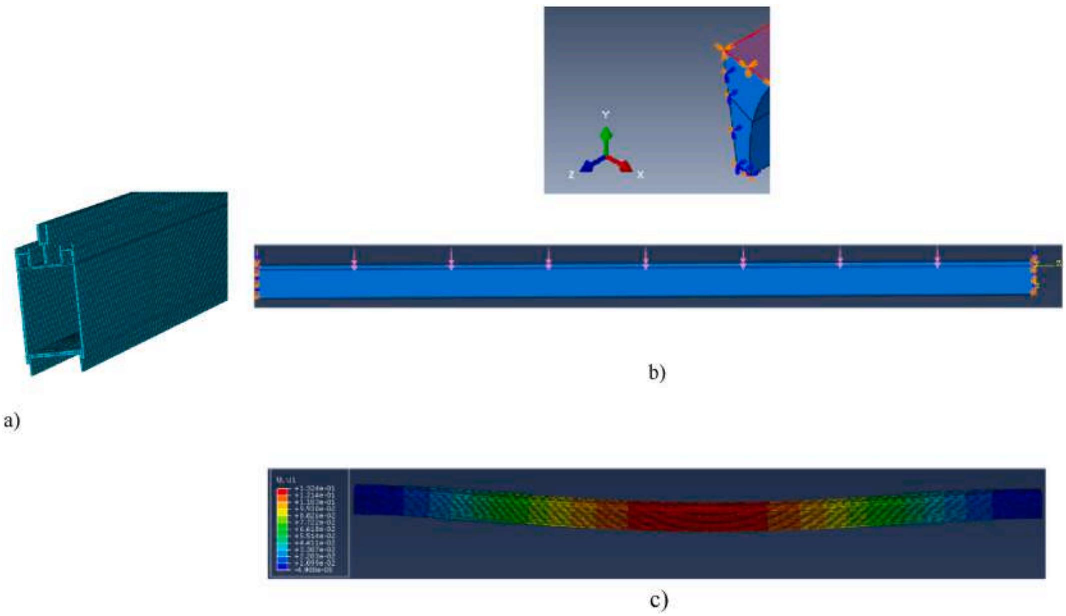

Fig. 10. Mesh (a), applied loading (b), and deformed configuration (c) of the aluminium alloy profile.

Fig. 10 illustrates the key elements of the numerical simulation setup used to analyze the baseline performance of the aluminum alloy profile prior to reinforcement.

Fig. 10(a) shows the finite element mesh employed in the numerical analysis. The mesh consists of elements with a side length of 5 mm, a dimension chosen based on a preliminary sensitivity study that balanced computational efficiency with solution accuracy. The turquoise-colored mesh clearly outlines the cross-sectional geometry of the aluminum profile, including its characteristic hollow chambers and internal reinforcing webs. The mesh density is consistent throughout the model, ensuring uniform accuracy across all critical regions.

Fig. 10(b) depicts the loading and boundary conditions applied in the simulation. The blue aluminum profile is supported at both ends (indicated by yellow supports), with a uniformly distributed load applied along the top surface (represented by red arrows). This loading scenario simulates a typical beam under a distributed load, common in architectural and structural applications. The coordinate system in the upper right corner sets the reference frame for the analysis, with the Y-axis corresponding to the vertical direction along which deflection is measured.

Fig. 10(c) presents the deformed configuration of the profile under the applied load, using a color gradient to represent deflection magnitude. The maximum deflection of 0.134 mm occurs at the midpoint of the span, as expected for a symmetrically loaded beam. The color spectrum ranges from blue (minimal deflection near the supports) to red (maximum deflection at the center), visually illustrating the deflection profile. This baseline deflection serves as the reference against which the performance enhancements of the various reinforcement configurations are evaluated.

Having established the baseline performance of the unreinforced profile (M0), the analysis then focused on the enhanced configurations (M1, M2, and M3) under identical loading conditions. The strengthened specimens were subsequently analyzed to quantify the benefits introduced by the prestressed steel reinforcement.

3.2. Performance of strengthened configurations

The detailed modeling of these configurations enabled precise analysis of stress distribution, deformation patterns, and overall structural behavior under applied loads. The mesh refinement visible in the models ensured accurate capture of localized effects, particularly at connection points between different materials and components. These numerical models were essential for evaluating the relative performance of each reinforcement strategy and identifying the most effective configuration (M2) prior to physical prototyping and testing. The level of detail in these models highlights the comprehensive approach taken in the numerical analysis phase of this research, providing a solid foundation for the subsequent experimental validation of the most promising configuration.

The cables in the steel-aluminum alloy composite sections M1, M2, and M3 were subjected to four levels of normal pre-tensile stress, calibrated as a percentage of the harmonic steel's nominal yield strength. The pre-tensioning values are set at 20 %, 30 %, 40 %, and 50 % of the steel's nominal yield strength.

Table 1 summarizes the results, presented in terms of maximum deflection at the midpoint of the profile. This table shows the percentage reduction in displacement compared to the maximum deflection of 0.134 mm observed in the M0 model.

Table 1 presents the percentage reduction in maximum deflection for the three different reinforced profile configurations (M1, M2, M3) compared to the unreinforced profile (M0), under varying levels of prestressing force. This data reveals several significant trends regarding the effectiveness of the reinforcement system.

At the lowest prestressing level (20 % of the steel's yield strength), there are notable differences in performance between the three configurations. The M2 model demonstrates a substantially higher deflection reduction (12.45 %) compared to M1 (2.04 %) and M3 (4.68 %). This indicates that the M2 configuration's anchoring system and wire arrangement provide superior stiffening effects even at lower prestressing forces. This makes it more efficient when lower prestressing levels are desired or necessary. As the prestressing force increases to 30 %, all configurations show marked improvement, but M2 still maintains its advantage (37.01 % reduction) over M3 (31.65 %) and M1 (18.81 %). The significant jump in performance between 20 % and 30 % prestressing suggests that there exists a threshold where the prestressing begins to contribute substantially to the composite system's stiffness.

At 40 % prestressing, the performance gap between configurations narrows, though M2 continues to lead with a 62.76 % deflection reduction compared to M3 (56.80 %) and M1 (45.85 %). This level represents a point where all configurations demonstrate high effectiveness, offering a good balance between performance and practical implementation.

Most remarkably, at the highest prestressing level (50 %), all three configurations achieve a similar exceptional performance, with deflection reductions exceeding 83 %. M1 slightly outperforms the others with an 87.24 % reduction, followed closely by M2 (86.18 %) and M3 (83.69 %). This convergence of performance at high prestressing levels suggests that when maximum stiffness is the primary goal, any of the three configurations could be suitable, with selection potentially based on other factors such as ease of installation or cost considerations.

Table 1
Analysis of prestressing effect on deflection reduction.

Pre-stressing force to cables [% of the steel f_0]	Model M1	Model M2	Model M3
20	2.04	12.45	4.68
30	18.81	37.01	31.65
40	45.85	62.76	56.8
50	87.24	86.18	83.69

The non-linear relationship between prestressing force and deflection reduction is particularly noteworthy. For instance, in the M2 configuration, doubling the prestressing force from 20 % to 40 % results in a five-fold increase in performance (from 12.45 % to 62.76 % deflection reduction). This non-linearity highlights the efficiency of higher prestressing levels in maximizing the composite system's stiffness. However, practical considerations regarding the long-term behavior of highly prestressed cables need to be addressed in future experimental work.

Fig. 11 presents a comparative graphical representation of the relationship between prestressing force and midpoint deflection for the three model configurations. The graph visually confirms and emphasizes several key findings from the numerical analysis.

While the numerical results provided valuable insights, experimental validation was essential to confirm the real-world applicability of the proposed reinforcement systems. An experimental testing campaign was conducted to verify the simulation outcomes, as detailed in the next section.

4. Experimental validation

The curtain wall profile chosen for laboratory experiments is made of aluminum alloy. It has a cross-section consisting of a 50 mm base and a height of 110 mm. It weighs 2827 kg/m, has a moment of inertia along the strong axis of 192.24 cm^4, and has a total length of 3000 mm. The mixed steel-aluminum member is obtained starting from the profile by inserting 4 straight cables, each with a diameter of 1 mm, which are kept in a straight position by means of a pair of cable holders, each of which is positioned at its ends, and are blocked, after being tensioned, by means of clamps. Fig. 12 shows some photos of the basic aluminium profile and of the one reinforced with steel cables before carrying out the experimental tests.

Fig. 13 shows the load system used for the profiles under investigation. It also shows the tubular systems equipped with circular end plates used to avoid the warping of the tested specimen.

The profiles were monitored during the test by means of a displacement transducer (LVDT) positioned at their midline to monitor the deflection and transducers near the supports to compute any rotations of the supports themselves. Strain gauges were also placed at the midline of the two vertical sides of the profile and on its upper base. The measuring instruments used are shown in Fig. 14.

4.1. Specimen Preparation

Difficulties in supplying steel cables with the diameter investigated in the numerical experimentation were encountered. This discrepancy in cable diameter (1 mm vs. 5 mm in simulations) introduces a significant deviation in stiffness and load-transfer behavior, which limits the direct comparability of experimental and numerical results. Moreover, the absence of precise tension control during testing further contributes to the observed inconsistencies in structural response. The CMS company was able to purchase only cables with a diameter of 1 mm on the market, a size much smaller than the diameter expected in the previous analysis phases. The aforementioned company carried out the cable pre-tensioning system without controlling the amount of the applied load. Therefore, it was not possible to precisely quantify the effect of the pre-compression induced on the aluminum profile by the presence of the steel cables. Furthermore, technical problems related to the unavailability of the test equipment delayed the execution of the experimental tests. Such unexpected waiting times inevitably contributed to increasing the relaxation effect of the steel cables, causing an increase in the tension drops in the steel systems, which reduces the beneficial effect of the induced pre-compression and, therefore, the effectiveness of the proposed mixed profile.

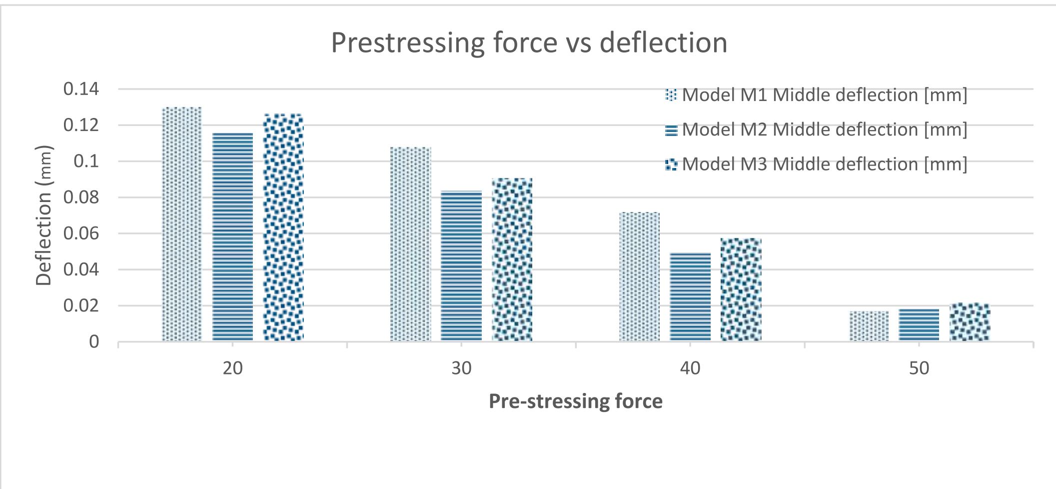

Fig. 11. Graphical Analysis of Prestressing Force vs. Deflection.

(a)

(b)

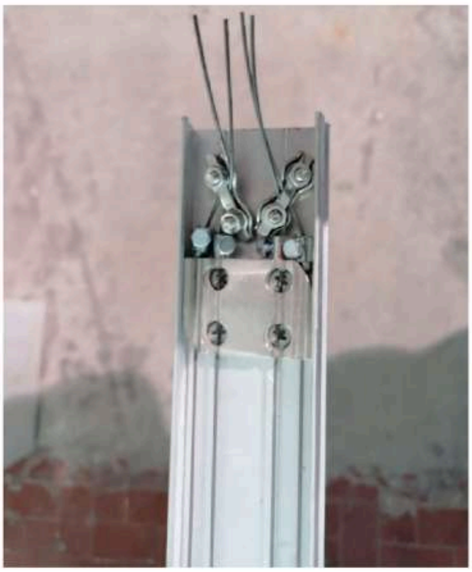

(c)

Fig. 12. The aluminium profile and the mixed steel-aluminium profile being tested (a, b) and detail of the cable locking clamps (c).

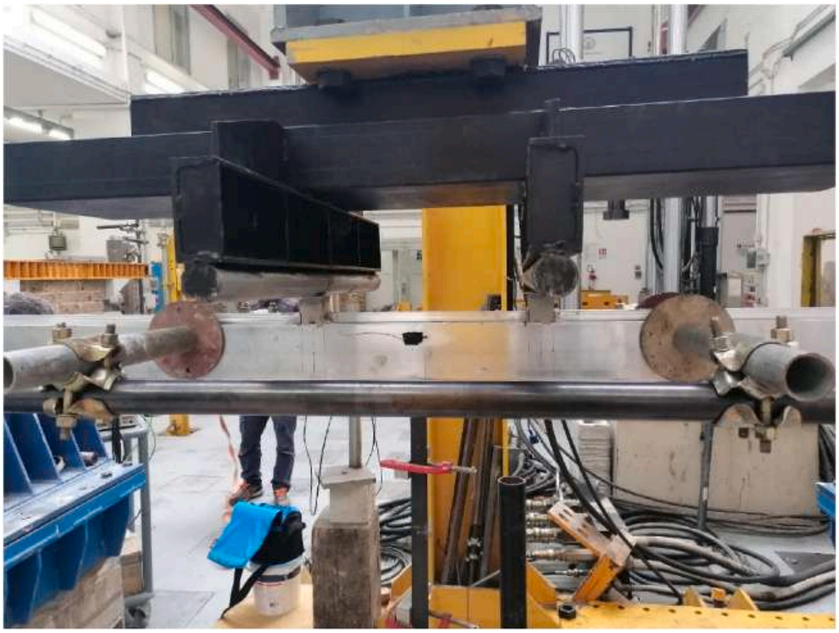

Fig. 13. Experimental setup: loading setup.

4.2. Quasi-static bending tests

Both profiles were subjected to 4-point bending tests. The supports were positioned at approximately 30 cm from the ends of the profiles to prevent the clamping clamps from coming into contact with the support cylinders, preventing the correct operation of the tensioned cables. Since the profile was equipped with end stiffeners on the lower base, a metal plate was welded in correspondence with the support areas to ensure a larger contact surface between the profile itself (Fig. 15). The load was applied to the members in two positions, spaced approximately 40 cm apart, using circular-section steel profiles connected to the actuator through a system of metal carpentry profiles. Considering that the aluminum profile has an upper base stiffened by several ribs of different heights, in order to allow uniform application of the load on a larger support area, the section of the profile was filled with high-strength pourable mortar produced by Mapei [35], which determined the creation of suitable support bearings for the load cylinders.

4.3. Observations on local instability and deflection

The experimental tests were conducted as a precautionary measure up to a maximum displacement of approximately 100 mm. However, the profiles showed deformation possibilities far more significant than those achieved experimentally, since at the maximum displacement reached, they did not exhibit any global failure mechanism (Fig. 16).

The only deformation mechanism revealed was the local instability of the stiffeners connected to the compressed flange of the profiles. This deformation mechanism, however, did not significantly reduce the members' resistance performance. It is visually reported in the two tested profiles in Fig. 17.

4.4. Comparison of experimental and numerical results

The diagrams resulting from the bending tests carried out on the two profiles are shown in Fig. 18. From this figure, although the tension applied to the cables is modest (some of them not being tensioned) and cannot be precisely quantified, the presence of the external pre-compression system used is able to reduce the deformation and increase the resistance of the profile by around 5 %.

Therefore, the results derived from this preliminary experimental campaign show the beneficial effect of the reinforcement system employed, which will undoubtedly be able to exhibit better performances in a future experimental campaign by increasing the tension applied to the cables (up to values 0.3–0.4 times their yield strength) and monitoring their tension drops until the moment of carrying out the load tests.

The experimental findings, in conjunction with the numerical results, form the basis for the following discussion on performance trends and practical implications. A critical analysis of both numerical and experimental outcomes is presented below to assess the overall effectiveness of the proposed solutions.

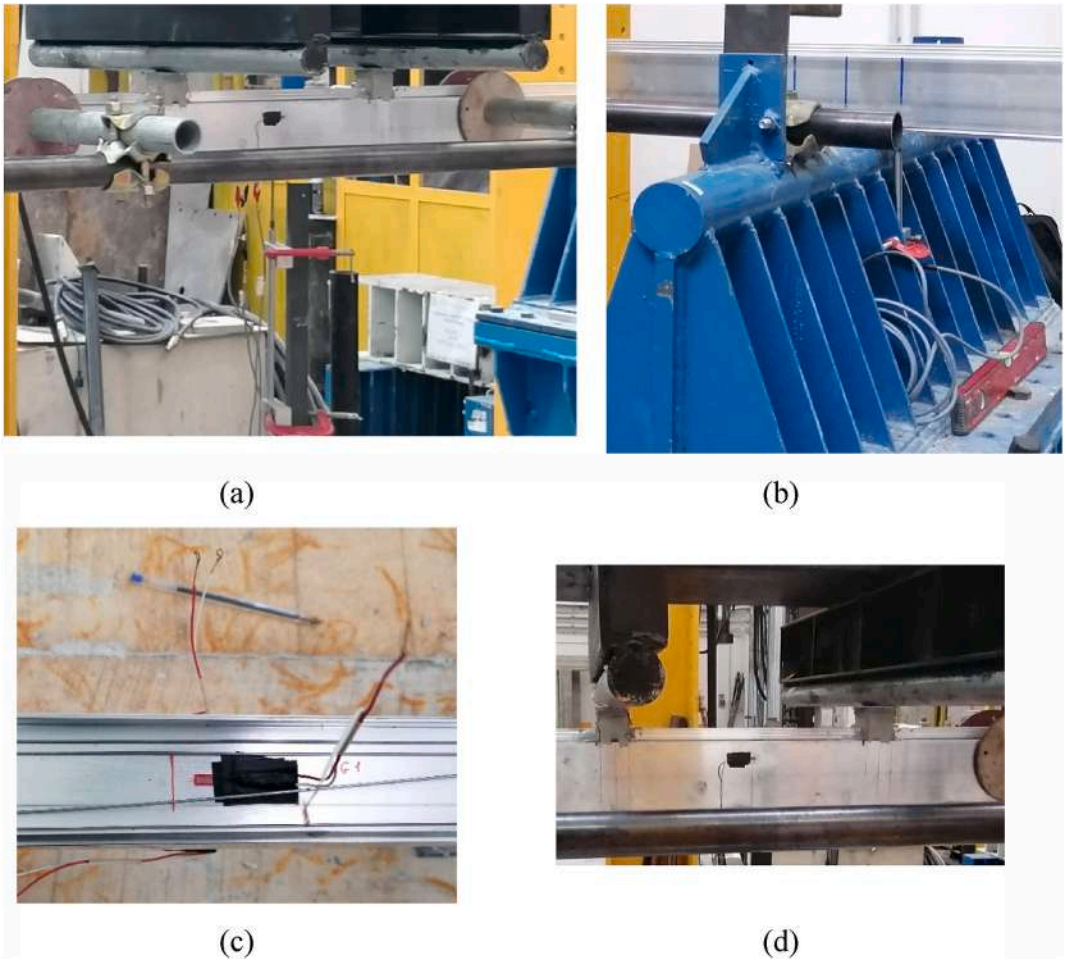

Fig. 14. Experimental setup: LVDT (a, b) and strain gauges (c, d).

Fig. 15. Experimental setup: support constraint.

5. Discussion

Overall, the results from numerical and experimental investigations demonstrate that all three reinforcement configurations, M1, M2, and M3, are capable of significantly enhancing the stiffness of aluminium curtain wall profiles, especially at higher prestressing levels. Among the configurations, the M2 profile consistently provides superior performance at low to moderate levels of prestressing, making it the most versatile and effective option across a range of applications.

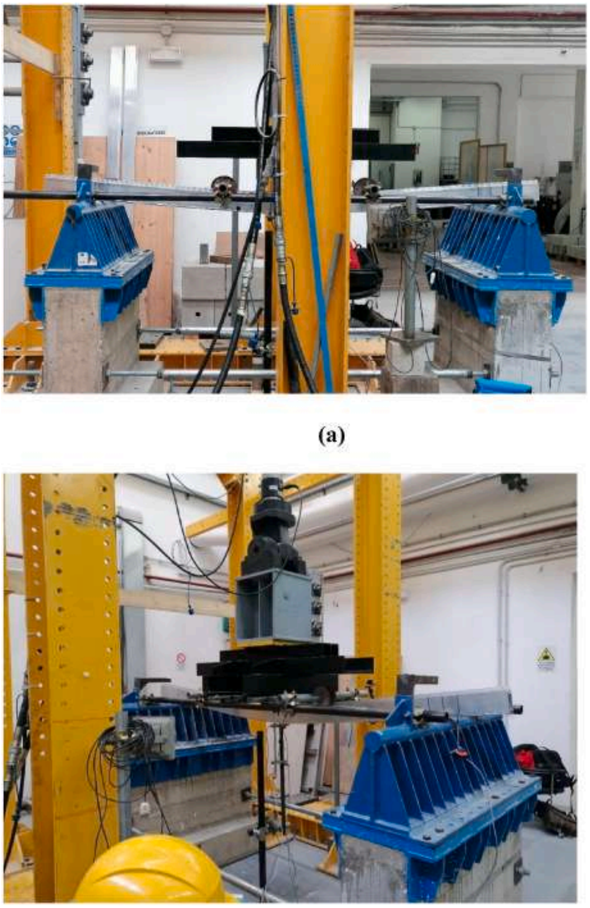

(a)

(b)

Fig. 16. Maximum deformation of the aluminium specimen (a) and of the reinforced specimen (b).

Fig. 17. Local instability phenomena in the experimentally tested profiles.

5.1. *Insights from numerical and experimental results*

The findings from the numerical analysis reveal that the midpoint deflection of the aluminium profile decreases non-linearly with increasing prestressing levels. At 50 % of the steel's nominal yield strength, all configurations achieve excellent performance, with

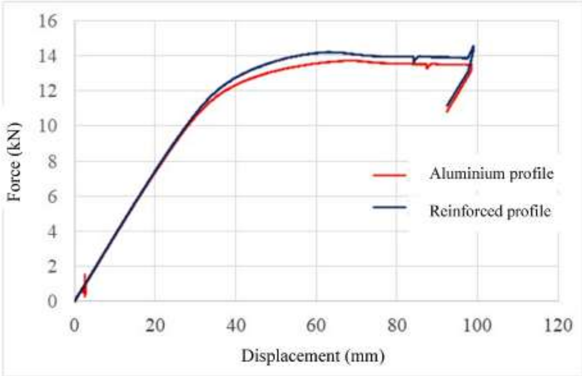

Fig. 18. Experimental comparison of the results of the bending tests performed on the two profiles.

deflection reductions exceeding 83 % compared to the unreinforced model.

While M2 generally outperforms M1 and M3 at lower and mid-level prestressing, the difference narrows at higher levels. This indicates that the choice of configuration may depend on practical factors such as ease of installation, material costs, or architectural constraints when high prestressing is feasible.

The experimental tests, although limited by the use of 1 mm cables (as opposed to the 4 mm ones used in simulations) and the inability to control the applied accurately prestress, still confirmed the beneficial effect of cable reinforcement on stiffness and load-bearing capacity. However, this mismatch in cable geometry and prestressing introduces scaling effects and stiffness deviations, reducing the accuracy of direct numerical-to-experimental comparisons. These limitations must be considered when interpreting the results, and they underscore the need for improved experimental control in future studies.

These combined results validate the effectiveness of the proposed composite system and provide a strong foundation for further study and implementation in real-world facade applications.

5.2. Practical implications

The proposed reinforced aluminium profile system offers a promising solution for curtain wall applications across diverse building types. The system's ability to enhance stiffness without increasing the visual impact of the profiles makes it particularly suitable for contemporary architecture, where large glass surfaces and minimal framing are desired, and for renovation projects, where performance upgrades must respect the original design intent.

The numerical results suggest that with 50 % prestressing, the reinforced profiles can achieve deflection reductions of more than 85 % compared to standard aluminum profiles, significantly expanding the application range of aluminum curtain wall systems.

Further, recent studies assess the structural performance of glass in facade applications. Naqash et al. [15,16] evaluates glass performance comprehensively, which is crucial for safety and durability in restoration projects. Their findings highlight the need to select materials and designs that meet aesthetic and structural criteria.

5.3. Proposed improvements and future directions

Future research directions will include.

1. Experimental validation through comprehensive laboratory testing
2. Long-term performance evaluation under cyclic loading and environmental exposure
3. Optimization of the prestressing technique for efficient industrial implementation
4. Integration with various glass and panel systems for different architectural applications
5. Economic and environmental analysis comparing the reinforced profile system with alternative solutions

This study contributes to the development of innovative solutions for high-performance building envelopes, offering a practical approach to enhance the structural performance of aluminium curtain wall systems while maintaining their aesthetic advantages. The versatility of the proposed system makes it applicable to a wide range of architectural contexts, from contemporary designs to renovation projects, potentially expanding the use of lightweight, sustainable aluminum systems in challenging applications.

This research initiates a broader investigation into prestressed aluminium systems. This work initiates a broader investigation into prestressed aluminium systems aimed at improving structural performance through cable-based reinforcement.

The insights gained from this study are synthesized in the concluding section, which outlines the main findings and suggests directions for future work. The conclusions drawn from this work highlight the structural benefits of the proposed reinforcement system and its potential applications.

While the experimental and numerical results showed good agreement in terms of global stiffness and load-deflection behavior, a detailed comparison of failure patterns is more challenging. Due to limitations in test documentation, consistent photographic evidence of failure for all specimens was not available, which restricted our ability to produce a direct visual comparison within a single figure, as suggested. However, the numerical simulations clearly indicated stress concentration zones and localized deformations, particularly near bolt holes, connector interfaces, and lateral flanges areas where visible damage and local buckling were qualitatively observed during physical testing. This correlation supports the validity of the numerical model in capturing the key failure mechanisms, despite the absence of one-to-one visual mapping. Future work will aim to improve experimental documentation to allow for more robust visual validation of simulation results.

6. Conclusions

This study investigated the behavior of steel-aluminum alloy composite sections under distributed loads resulting from lateral actions, with a focus on innovative prestressed profiles for curtain wall systems. The primary objective was to evaluate the effectiveness of prestressed steel cables in enhancing the structural performance of aluminum mullions.

Prestressed configurations (M1, M2, and M3) demonstrated significant reductions in deflection compared to the unreinforced profile (M0). Among the configurations, the M2 profile consistently provided the best performance across various prestressing levels, achieving up to an 86 % reduction in deflection under a 50 % prestressing force.

Preliminary laboratory tests confirmed the beneficial effects of prestressing, with the reinforced profiles exhibiting improved stiffness and load-bearing capacity. Local instability phenomena observed in the experimental tests were minor and did not compromise the overall structural performance.

The proposed system offers a practical and aesthetically viable solution for modern and historical curtain wall applications, addressing both structural and architectural requirements. The versatility of the M2 configuration makes it suitable for a wide range of building types, particularly in high-rise projects.

Future studies should focus on optimizing the prestressing technique, conducting long-term durability tests, and exploring the integration of the system with advanced glass and panel materials. The economic and environmental aspects of the proposed reinforcement system should also be evaluated to ensure its feasibility for large-scale implementation.

It should be noted that the experimental profiles were reinforced with smaller-diameter cables (1 mm) than those used in the numerical models (4 mm), and the prestressing force was not precisely controlled. These factors limit the full comparability between experimental and numerical outcomes. Future experimental campaigns will address this by using matching cable sizes and calibrated prestress levels to ensure more accurate validation.

In conclusion, the proposed prestressed aluminum profiles represent a significant advancement in curtain wall technology, offering a balanced solution for enhancing structural performance while preserving architectural integrity.

Nomenclature

Symbol/Term	Description
AW-6060 T5	Aluminium-magnesium-silicon alloy used for the base profile
ABAQUS	Finite Element Analysis software used for numerical modeling
M0	Unreinforced aluminium profile (baseline model)
M1, M2, M3	Reinforced composite aluminium profiles with different cable configurations
$\mathbf{f_{0\cdot 2}}$	Conventional yield strength of aluminium (MPa)
$\mathbf{f_u}$	Ultimate tensile strength (MPa)
$\mathbf{A_{50}}$	Elongation at fracture over 50 mm gauge length (%)
$\mathbf{f\_R_0}$	Nominal yield strength of harmonic steel cables (MPa)
p	Applied uniform pressure simulating wind load (MPa)
E	Young’s modulus (elastic modulus)
TSPEI	Countersunk hex screws used in the M1 configuration
DIC	Digital Image Correlation, used for strain/displacement measurements
LVDT	Linear Variable Displacement Transducer, for measuring deflections
Prestressing Level	Percentage of the steel’s yield strength applied as pretension in the cables
Deflection	Vertical displacement of the profile under load (mm)
NTC 2018	Italian Technical Standards for Construction
Eurocode 9	European standard for the design of aluminium structures
S275	Grade of steel used for rope supports
MPa	Megapascal (unit of pressure/stress)

CRediT authorship contribution statement

Antonio Formisano: Writing – review & editing, Writing – original draft, Visualization, Validation, Supervision, Software, Resources, Project administration, Methodology, Investigation, Funding acquisition, Formal analysis, Data curation, Conceptualization. **Muhammad Tayyab Naqash:** Writing – review & editing, Writing – original draft, Software, Resources, Investigation, Formal analysis.

Ethics approval and consent to participate

There are no ethical conflicts, and consent was obtained from all participants involved in the study. They were informed about the purpose of the study, the potential risks and benefits, and their right to withdraw at any point without consequences.

Consent for publication

We have obtained consent from all participants in the study to publish individual data, images, or any other identifiable information.

Availability of data and materials

The data and materials are within the paper itself. Any additional information can be obtained by contacting one of the authors.

Funding

"No funding was obtained for this study".

Declaration of competing interest

The authors declare the following financial interests/personal relationships which may be considered as potential competing interests: Antonio Formisano reports was provided by University of Naples Federico II. If there are other authors, they declare that they have no known competing financial interests or personal relationships that could have appeared to influence the work reported in this paper.

Acknowledgments

The authors would like to acknowledge the company Costruzioni Metalliche Santonicola Srl for financing the present research activities within the framework of a research contract with the Department of Structures for Engineering and Architecture at the University of Naples Federico II (Scientific Supervisor: A. Formisano).

Data availability

Data will be made available on request.

References

[1] M.T. Naqash, Design and fabrication of aluminum cladding and curtain wall of a sports club, Open J. Civ. Eng. (2019), https://doi.org/10.4236/ojce.2019.91001.
[2] M.T. Naqash, A. Formisano, Assessment of cantilevered curtain wall system supported by tension rods for an enclosed circular building, Structures 68 (May) (2024) 107133, https://doi.org/10.1016/j.istruc.2024.107133.
[3] A. Pisapia, E. Nastri, V. Piluso, A. Formisano, F. Massimo Mazzolani, Experimental campaign on structural aluminium alloys under monotonic and cyclic loading, Eng. Struct. (2023), https://doi.org/10.1016/j.engstruct.2023.115836.
[4] F.M. Mazzolani, V. Piluso, G. Rizzano, Local buckling of aluminum alloy angles under uniform compression, J. Struct. Eng. 137 (2) (2011), https://doi.org/10.1061/(asce)st.1943-541x.0000289.
[5] Building façade design: 3 applications starring aluminium. https://blog.almecogroup.com/building-facade-design-3-applications-starring-aluminium/. (Accessed 8 October 2024).
[6] S. Bose, Restoration of Town Hall in Kolkata for adaptive reuse: a case study, Struct. Surv. 30 (3) (2012), https://doi.org/10.1108/02630801211241838.
[7] S.A. Moghaddam, C. Serra, M. Gameiro da Silva, N. Simões, "Comprehensive review and analysis of glazing systems towards nearly zero-energy buildings: energy performance, thermal comfort, Cost-Effectiveness, and Environmental Impact Perspectives (2023), https://doi.org/10.3390/en16176283.
[8] C. Clifton, M. Bruneau, G. MacRae, R. Leon, A. Fussell, Steel structures damage from the Christchurch earthquake series of 2010 and 2011, Bull. N. Z. Soc. Earthq. Eng. (2011), https://doi.org/10.5459/bnzsee.44.4.297-318.
[9] C.D. Clift, N. Bonnheim, Design of curtain walls for wind load, in: Curtain Wall Systems, A Primer, 2013, https://doi.org/10.1061/9780784412701.ch07.
[10] S. Dogru, F. Cakir, B. Akbas, Structural evaluation of unitized curtain wall systems by using inter-story drift test, Challenge Journal of Structural Mechanics (2022), https://doi.org/10.20528/cjsmec.2022.01.003.
[11] M.T. Naqash, A. Formisano, G. De Matteis, Aluminium framing members in facades, in: Key Engineering Materials, 2016, https://doi.org/10.4028/www.scientific.net/KEM.710.327.
[12] N.M. Tayyab, A. Formisano, D.M. Gianfranco, Design and performance testing of a skylight in Qatar, in: Key Engineering Materials, 2016, https://doi.org/10.4028/www.scientific.net/KEM.710.262.
[13] A. Formisano, M.T. Naqash, Composite aluminium-steel curtain walls for refurbishment of historical buildings: proposed solution and preliminary experimental tests, Lecture Notes in Civil Engineering 595 (LNCE) (2025) 340–347, https://doi.org/10.1007/978-3-031-87312-6_42.
[14] T. Saroglou, T. Theodosiou, B. Givoni, I.A. Meir, Studies on the optimum double-skin curtain wall design for high-rise buildings in the Mediterranean climate, Energy Build. (2020), https://doi.org/10.1016/j.enbuild.2019.109641.
[15] W.Y. Cai, J. Jiang, G.Q. Li, Y.B. Wang, Fracture behavior of high-strength bolted steel connections at elevated temperatures, Eng. Struct. (2021), https://doi.org/10.1016/j.engstruct.2021.112817.
[16] M. Khelifa, A. Khennane, M. Oudjene, Modelling of strengthened steel connections under static and cyclic loading, Buildings (2022), https://doi.org/10.3390/buildings12111962.

[17] W. Mansour, B. Osama, W. Li, P. Wang, M.H.R. Sobuz, Numerical response of concrete-filled steel tubular (CFST) columns externally strengthened with FRP composites subjected to cyclic loading, Int J Concr Struct Mater 18 (1) (Dec. 2024), https://doi.org/10.1186/s40069-024-00716-6.
[18] S. Abu Dabous, T. Ibrahim, S. Shareef, E. Mushtaha, I. Alsyouf, Sustainable façade cladding selection for buildings in hot climates based on thermal performance and energy consumption, Results Eng. (2022), https://doi.org/10.1016/j.rineng.2022.100643.
[19] B. Gligić, D. Budevać, Z. Marković, Z. Mišković, Aluminium alloy girders strengthened by steel elements, Gradjevinar 68 (10) (2016) 787–799, https://doi.org/10.14256/JCE.1588.2016.
[20] A.D. Lee, P. Shepherd, M.C. Evernden, D. Metcalfe, Optimizing the architectural layouts and technical specifications of curtain walls to minimize use of aluminium, Structures (2018), https://doi.org/10.1016/j.istruc.2017.10.004.
[21] M.T. Formisano Antonio, Naqash, Numerical studies on innovative prestressed aluminium alloy profiles for curtain Wall systems, in: V, N. E, F.A. Mazzolani, M. Federico, Piluso (Eds.), Proceedings of the 11th International Conference on Behaviour of Steel Structures in Seismic Areas, Springer Nature Switzerland, Cham, 2024, pp. 863–871.
[22] M.T. Naqash, S. Khoso, E. Noroozinejad Farsangi, Wind-Induced structural response of skylights: a eurocode-based assessment, in: Practice Periodical on Structural Design and Construction, 2024, https://doi.org/10.1061/ppscfx.sceng-1381.
[23] The brand - who are we | Technal Middle East. https://www.technal.com/en/tme/the-brand/. (Accessed 10 October 2023).
[24] BS EN 1993-1-1, BS EN 1993-1-1:2005+A1:2014 Eurocode 3 - Design of Steel Structures - Part 1-1: General Rules and Rules for Buildings, 2014.
[25] EN 1990-1: EC0, EN 1990-1: Eurocode 0 - Basis of Structural Design," EU, Regulation 305/2011, 2002.
[26] European-Union, Eurocode 9: Design of Aluminium Structures - Part 1-1 : General Structural Rules, European Committee for Standardization, 2007.
[27] P.S. Bulson, Aluminium structures - a guide to their specifications and design, Eng. Struct. (1996), https://doi.org/10.1016/s0141-0296(96)90020-6.
[28] H.E.R. Lake, Aluminium structures - a guide to their specifications and design, in: J.R. Kissell, R.L. Ferry (Eds.), Strain, 1996, https://doi.org/10.1111/j.1475-1305.1996.tb00989.x.
[29] A. Duval, et al., Abaqus/CAE 6.14 User's Manual, Dassault Systémes Inc., Providence, RI, USA, 2014.
[30] R. Gitter, Design of Aluminium structures: selection of Structural Alloys, in: Paper Presented at the Workshop in Brussels: EUROCODES - Background and Applications, 2008. *Brussels*.
[31] C.M. Database, et al., Abaqus/CAE 6.11 User's Manual, Dassault Systémes Inc., Providence, RI, USA, 2011.
[32] G. De Matteis, M.T. Naqash, G. Brando, Parametric analysis of welded aluminium T-Stub connections parametric analysis of welded aluminium T-Stub connections, in: Environmental Engineering, 2011, pp. 311–327.
[33] I. M. of I. and NTC, Norme Tecniche per Le Costruzioni, Gazzetta Ufficiale della Repubblica, Italiana, 2018. DM 17/1/2018.
[34] NTC 2018, Norme Tecniche per Le Costruzioni, Italian Standard.," Rome, 2018.
[35] Concrete Repair Mortar Solutions | MAPEI System Solutions | Mapei. https://www.mapei.com/us/en-us/products-and-solutions/in-the-spotlight/concrete-repair-mortars. (Accessed 28 June 2025).